JOURNAL OF PROPULSION AND POWER
Vol. 18, No. 1, January–February 2002

Integrated Design and Analysis of Intakes and Nozzles in Air-Breathing Engines

M. Ferlauto,* F. Larocca,† and L. Zannetti‡
Politecnico di Torino, 10129 Turin, Italy

A numerical technique is described for the design and analysis of the flow in air intakes and nozzles. The design concept is considered as an integrated design in which the nozzles and intake are parts that communicate with the system as a whole. The unsteady Euler equations are numerically integrated using a time-dependent procedure and adopting a finite volume approximation. In analysis mode, simple models simulate the components linking intake and nozzles, that is, compressor, combustor, and turbine. The external flow, intake, and nozzle flows are then computed simultaneously. In design mode, the procedure used to fit plume interfaces is also used to solve an additional inverse problem and to find the nozzle (or intake) shape that matches a prescribed pressure distribution at the wall. The procedure is explained through several numerical examples of increasing complexity.

Nomenclature

$b(x,t)$, $c(x,t)$	=	lower and upper boundary curves of the computational domain
c_p	=	specific heat at constant pressure
D	=	domain in $(x, y) \in R^2$
e	=	total internal energy per unit of volume
$\boldsymbol{i}, \boldsymbol{j}$	=	unit vectors
$\boldsymbol{F}, \boldsymbol{G}$	=	flux vectors
h^0	=	total enthalpy per unit of volume
L_{ref}	=	reference length
M	=	Mach number
$\boldsymbol{N}$	=	vector of source terms
$\boldsymbol{n}$	=	normal unit vector
p	=	pressure
p^0	=	total pressure
p^0_{ref}	=	reference total pressure
Q	=	heat per unit of mass
T^0	=	total temperature
T^0_{ref}	=	reference total temperature
T^0_t	=	total temperature prescribed along the burner
t	=	time
$\boldsymbol{U}$	=	vector of conservative variables
u, v	=	Cartesian velocity components
x, y	=	Cartesian coordinates
γ	=	ratio of specific heats
Δ	=	difference
δ	=	inlet ramp angle
∂D	=	boundary of D
θ	=	burner parameter
ρ	=	density
τ_b	=	ratio of burner total temperatures

Subscripts

bi	=	burner inlet
bo	=	burner outlet
in	=	inlet
ou	=	outlet
ref	=	reference value
w	=	wall
∞	=	freestream

Received 22 April 2000; revision received 11 December 2000; accepted for publication 8 July 2001.

*Research Associate, Dipartimento di Ingegneria Aeronautica e Spaziale, Corso Duca degli Abruzzi 24; ferlauto@athena.polito.it. Member AIAA.

†Assistant Professor, Dipartimento di Ingegneria Aeronautica e Spaziale, Corso Duca degli Abruzzi 24; larocca@polito.it.

‡Professor, Dipartimento di Ingegneria Aeronautica e Spaziale, Corso Duca degli Abruzzi 24; zannetti@polito.it. Member AIAA.

I. Introduction

In design practice, an air-breathing engine is generally split into many subsystems, which are then studied separately. The links between each subsystem consist of an appropriate boundary condition, gathered from design experience[1] and then updated through an iterative process based on direct analyses. The iterative process continues until the design goals are reached. A critical point in this procedure is the design of nozzles and air intakes, which represent the links between the inner flowfield of the engine and the external flow. Unlike other engine subsystems, the operative range of such devices is too wide to be summarized by empirical correlations, and interferences with the external flow can lead to very complex flow phenomena.

Nozzles and air intakes are very sensitive to external flowfield interactions. For instance, in the afterbody region, the presence of flows with different thermodynamic properties gives rise to shear layers that interact with each other in an a priori unpredictable scenario. Compressibility effects are also of relevance, so that interferences with other flow discontinuities, either as shocks or expansion waves, must be taken into account.

The sensitivity to the external airflow is even more pronounced for highly integrated engines, as in hypersonic propulsion,[2,3] because of the higher coupling between the propulsion system flowfield and the vehicle aerodynamics. The natural consequence of the factors mentioned earlier is an increase of installation drag, which in turn reduces the net thrust.[4]

Nevertheless, reasons such as performance enhancements, noise reduction, and minimization of operative cost, push designers toward highly integrated propulsion systems, for which a more careful design of expansion and compression systems is required. In recent years engine/airframe integration has become a relevant design branch,[3] in which numerical tools are extensively used to investigate design and offdesign operating conditions.

The present paper shows the feasibility of a one-shot numerical procedure for the evaluation of the internal and external flows past an entire air-breathing propulsion system. Some of the internal components such as the compressor, combustor, and turbine can be modeled by black-box models, whereas the internal inlet, fan and nozzles flows, and external flows are computed simultaneously.

The present formulation is designed as an economical tool with a prudent use of computational resources. On one hand, it is intended as an academic demonstration of a procedure that aims at more ambitious and realistic engine flow simulations. On the other hand, it can be considered, at the present stage, as a useful means to provide a fast estimate of the whole flow past a propulsion system.

With such a guideline in mind, the flow has been assumed as inviscid and two dimensional or axisymmetric. The inviscid flow assumption allows the use of coarse grids, thus avoiding the need of fine grids for boundary and mixing layer resolution. The two-dimensional or axisymmetric assumption obviously offers grid saving, but the present inviscid formulation can be straightforwardly extended to a three-dimensional formulation, as can be inferred from the three-dimensional version of the here adopted inverse procedure.[5]

Moreover, as described in some detail in Sec. III, the interface fitting between different flows is consistent with the inviscid flow assumption and, besides high accuracy, guarantees a further reduction of the number of grid points. Such model simplifications has allowed the numerical examples presented to be carried out on a 300-MHz Pentium personal computer.

The extension to three-dimensional viscous flow computations is not direct; it implies grid refinement in the boundary and shear layers and possibly adaptive refinement in the mixing regions, where different flows interact. Nevertheless, the present formulation may provide a good estimate of the location of mixing layers for the grid definition of viscous computations. The approach proposed is a natural extension of classical design tools as inverse methods[5–7] to a class of problems where flow discontinuities and mutual interferences play a major role in determining performances.

In inverse problems, the designer prescribes some flow properties and then solves them for the wall geometry that satisfies the imposed flow features. Let us consider the design datum to be a pressure distribution that has to be obtained along a solid boundary. The problem is solved by replacing the selected wall with a deformable and impermeable surface, an initial shape is assumed, and then design pressure and impermeability are imposed as boundary conditions. During the transient, the shape of such a surface changes to accommodate the flowfield, until a steady state is reached. The same model can be used to define the geometry of the fluid interfaces, which are material surfaces with the same pressure on their sides. The use of shock-capturing techniques ensures that the interactions between the flow discontinuities are accounted for.

Furthermore, the flow around the complete engine can be considered by adopting simplified models or black-box systems to simulate devices such as the burner, the compressor, and turbine stages. This assumption is generally valid because the timescales associated to the unsteadiness in such devices, that is, chemical reactions or energy conversion processes, are quite different, when compared with the unsteady response of inlets and nozzles to the external flow. Therefore, the dynamics of the whole system can be reproduced by simulating the flow entering the air intakes, the exchange of heat and work within the black-box systems, flow through the nozzles, and interactions with the external airflow region.

The paper is set out as follows: In the next section, the mathematical model and numerical procedure are illustrated. The technique is first applied to the design of a dual nozzle configuration interacting with the plumes. A test concerning a turbofan–nacellelike configuration is then shown as an example of the analysis of flows with multiple fluid interfaces. Finally, a ramjet model is formulated in which the air-intake flowfield is linked to a nozzle flowfield through a black-box model of the combustor that simulates the heat addition.

II. Mathematical Model

We formulate an inverse problem in which the location of the contact interfaces is not known a priori, and their final shape is part of the solution. At the same time, other design requirements, expressed in terms of pressure distributions, can be prescribed to obtain the desired nozzle performances. Further enhancements can be obtained by coupling the inverse problem with classical optimization procedures, such as the adjoint technique, to minimize or maximize a given objective functional.[8] The design problem of finding the shapes of intakes or nozzles that satisfy the prescribed pressure distributions is here solved according to a time-dependent process.[5,6] Interfaces that separate internal flows are fitted, as in the jet of multiple nozzles and the external flow, whereas shocks or contact discontinuities inside each flow are inherently captured by the numerical scheme. From the numerical point of view, the method is based on the finite volume projection of the time-dependent Euler equations according to a second-order accurate essentially nonoscillatory (ENO) scheme.[9]

A. Governing Equation

The Euler equations for the two-dimensional or axisymmetric unsteady motion of an inviscid compressible fluid are written in divergence form:

$$\frac{\partial \boldsymbol{U}}{\partial t} + \frac{\partial \boldsymbol{F}}{\partial x} + \frac{\partial \boldsymbol{G}}{\partial y} = -\alpha \frac{\boldsymbol{N}}{y} \tag{1}$$

where $\alpha = 0$ for a two-dimensional flow and $\alpha = 1$ for an axisymmetric flow, and

$$\boldsymbol{U} = \begin{Bmatrix} \rho \\ \rho u \\ \rho v \\ e \end{Bmatrix}, \qquad \boldsymbol{F} = \begin{Bmatrix} \rho u \\ p + \rho u^2 \\ \rho uv \\ (e + p)u \end{Bmatrix}$$

$$\boldsymbol{G} = \begin{Bmatrix} \rho v \\ \rho uv \\ p + \rho v^2 \\ (e + p)v \end{Bmatrix}, \qquad \boldsymbol{N} = \begin{Bmatrix} \rho v \\ \rho uv \\ \rho v^2 \\ (e + p)v \end{Bmatrix} \tag{2}$$

All of the flow properties are normalized to the reference values p^0_{ref}, T^0_{ref}, and L_{ref}. The reference quantities normally coincide with the freestream ones. According to the Gauss formula, the integral of Eq. (1) in a given volume D in space can be written as

$$\frac{\partial}{\partial t}\int_D \boldsymbol{U}\,\mathrm{d}\mathcal{V} + \int_{\partial D} (\boldsymbol{Fi} + \boldsymbol{Gj}) \cdot \boldsymbol{n}\,\mathrm{d}\sigma = -\alpha \int_D \frac{\boldsymbol{N}}{y}\,\mathrm{d}\mathcal{V} \tag{3}$$

Equation (3) is approximated using a finite volume technique by discretizing the domain D with four-sided cells whose shape depends on time. The integration in time is carried out according to a Godunov-type two-step scheme (see Ref. 10). A standard first order flux difference splitting (FDS) is used at the predictor step: The primitive variables (ρ, p, e, u, v) are assumed as an averaged, constant value inside each cell. The fluxes $\boldsymbol{F}$ and $\boldsymbol{G}$ are evaluated by solving the Riemann problems pertinent to the discontinuities that take place at the cell interfaces. For this purpose, the approximate Riemann solver suggested by Pandolfi[11] was adopted. At the corrector level, second order of accuracy is achieved by assuming a linear, instead of constant, behavior of the primitive variables inside the cells, according to the ENO concept.[9] The resulting scheme is second-order accurate in both time and space.[10]

B. Boundary Conditions

The computation at the boundaries is carried out by solving a half Riemann problem, as described by Larocca and Zannetti.[7] Briefly, in the same spirit as the FDS method used at the internal cells interfaces,[11] the boundary fluxes are evaluated from a combination of boundary conditions and wave-system signals that reach the border from inside. The number of conditions that has to be given at the boundary is, therefore, prescribed by the number of characteristic lines irradiated from the border toward the inner field, whereas their quality is dictated by the physics of the problem that has to be solved.

The computational domain is bounded by artificial contours, for example, far-field or permeable boundaries such as inlet and outlet, and physical contours, for example, impermeable walls. Three boundary conditions are needed at the subsonic inlet. Total pressure,

total temperature, and the flow angle have been imposed. In the supersonic case, all of the flow variables are prescribed. Conversely, one boundary condition is needed for subsonic flows at the outlet, whereas none is needed for supersonic flows. Usually the static pressure is prescribed at subsonic outlets. One boundary condition is needed at the walls. At solid walls, the impermeability imposes the vanishing of the normal velocity component. According to the inverse problem formulation, the design pressure is prescribed at flexible walls. The impermeability condition determines the evolution in time of the wall shape. In fact, to prevent a flux through the border, the wall has to move with a velocity equal to the normal component of flow velocity. At each time step, the grid is adjusted to fit the updated wall geometry. As an example, let us consider a channel that in a Cartesian x, y reference frame is bounded by two inlet and exit permeable boundaries $x = x_{in}$ and $x = x_{out}$ and by two impermeable flexible walls $y = b(x, t)$ and $y = c(x, t)$. A boundary-fitted grid can be defined by the $\xi = \text{const}$ and $\eta = \text{const}$ coordinate lines of the ξ, η reference frame defined by the mapping

$$\xi = \frac{x - x_{in}}{x_{ou} - x_{in}}, \qquad \eta = \frac{y - b(x,t)}{c(x,t) - b(x,t)} \tag{4}$$

The impermeability of the walls is then expressed by the kinematic conditions

$$\frac{\partial b}{\partial t} = v - u\frac{\partial b}{\partial x}, \qquad \frac{\partial c}{\partial t} = v - u\frac{\partial b}{\partial x} \tag{5}$$

Once $\partial b/\partial x$ and $\partial c/\partial x$ are approximated by finite differences, the new wall shapes $y = b(x, t + \Delta t)$ and $y = c(x, t + \Delta t)$ are updated by integrating Eqs. (5), and a new grid is determined according to the mapping (4). A more detailed description of this procedure can be found by Zannetti.[6]

The same inverse method can be used to determine the shape of plumes and interfaces. For instance, the stream tube confining a jet in still air may be viewed as the wall of a duct along which a constant pressure is prescribed. Moreover, in flow regions, such as after bodies or dual nozzles in a by-pass turbofan, contact discontinuities are generated by the different stagnation conditions and thermodynamic properties of the incoming flows. Such discontinuities are interfaces that can be explicitly computed according to the present inverse method: are considered as impermeable and deformable boundaries that separate different flow regions, across which pressure and the normal component of the flow velocity are imposed to be C^0 continuous and equal to the deformable boundary velocity, as dictated by the physics of contact discontinuities in inviscid flows. The pressure continuity provides the boundary condition that allows the flow to be computed on the two sides of the interface, whereas the normal flow velocity defines the interface shape evolution, as in the earlier described inverse problem.

To simulate the presence of components such as the burner, the turbine, and compressor stages, the use of simplified models or black boxes has been recalled. Any properly defined and physically correct model, based either on theoretical or on experimental work, is of course acceptable. It is not the scope of this work to enter into the merit of such models. Nevertheless, a burner model is described in Sec. IV.C. The turbine and compressor stage can also be modeled by actuator disks[12] or by simulating the blade presence through the volume forces.[13]

III. Accuracy and Validation

Some considerations on the accuracy and the validation of the proposed technique are made. Let us first describe the general philosophy that was followed to select the computational method. Once an inviscid flow model was selected, we looked for a technique that provides a numerical approximation with the best possible compromise between simplicity and accuracy. When dealing with inviscid compressible flows, the main difficulties are encountered for the description of discontinuities, such as shock waves and contact discontinuities. Since the 1960s, when the value of computational fluid dynamics (CFD) began to be asserted as a valuable practical and theoretical tool, controversy has arisen in the scientific community between the followers of the shock-fitting and the shock-capturing schools. The followers of shock fitting based their methods on the explicit treatment of flow discontinuities and were capable of obtaining quite accurate results with poor grids, without the wiggles that plagued the computations of followers of shock capturing, who, on the other hand, stressed the incomparably greater simplicity of their conservative approaches.

CFD for compressible flows has undergone great improvements over the years. Upwinding, total variation diminishing, ENO concepts have been introduced so that the quality of the results obtained using the conservative methods has dramatically increased. Even though the accuracy of a shock-fitting method cannot be matched, modern conservative methods have become as almost universal tools to describe numerically compressible flows affected by discontinuities. Their main advantage is simplicity, whereas the main drawback is the spreading of discontinuities over a certain number of grid points.

To recover resolution power, a conservative method needs more refined grids than a discontinuity-fitting method. Such a drawback is much more significant for contact discontinuities than for shock waves. The ability of up-to-date conservative methods to contain the spreading of a shock wave over a few meshes in fact fails for contact discontinuities. An intuitive explanation for this difficulty is that a shock wave is characterized by pressure waves propagating along converging characteristics, whereas a contact discontinuity is characterized by different flow properties advected along the discontinuity by parallel characteristics. The convergence of characteristics on shock waves provides a mechanism that opposes numerical diffusion and that is not present in the contact discontinuity case.

The flows we are interested in are in general affected by a complicated system of discontinuities, such as shock waves in supersonic flow regions, contact discontinuities due to shock interactions, and contiguity of different flows. Our choice is the use of a modern conservative method to capture shock waves and their interactions inside single flows, while the interfaces between the different flows are fitted. In this manner a good compromise between accuracy and simplicity can be expected. The fitting of the inner discontinuities is in fact not feasible, due to their complicate geometry and unpredictable nature, whereas the fitting of the interfaces between different flows is here implemented in the simple framework of a general inverse procedure. The obtained advantage is high resolution without the need of interface grid refinement and avoidance of numerical artifacts such as spurious diffusion.

The proposed method has been validated through comparison with analytical, numerical, and experimental results. The authors believe that the most significant test to validate a Euler code is a comparison with analytical solutions because good agreements with experimental results may be due to chance agreement between the numerical and physical viscosity. The comparison with other numerical methods may also be unreliable. Unfortunately there are few significant analytical solutions of the Euler equations for compressible flows; therefore, the Ringleb flow (see Ref. 6) was assumed as a meaningful benchmark to validate our inverse method. The method has also been checked with experimental results and compared to other numerical methods.

As far as the comparison to the analytically known Ringleb flow is concerned, a test is presented in Ref. 6. A channel formed by two streamlines of the Ringleb flow was solved as an inverse problem, that is, the theoretical pressure along two streamlines was assumed as datum to design the walls of a channel; the computed flowfield and wall shape were then compared to the analytically known solution. The selected streamlines were such that the flow was transonic with transition from subsonic to supersonic flow. In spite of the very poor grid (19×7) used, the relative error in the wall shape and flow Mach number was $\mathcal{O}(10^{-3})$. A much more severe test on the present formulation of the inverse method is shown in Ref. 7, in which the same Ringleb transonic channel is also computed in reverse flow, that is, with a shockless transition from supersonic to subsonic flow. The relative error in this case is $\mathcal{O}(10^{-2})$. A validating comparison of the results of the present method with experimental and numerical results has been made as part of the work organized by the AGARD

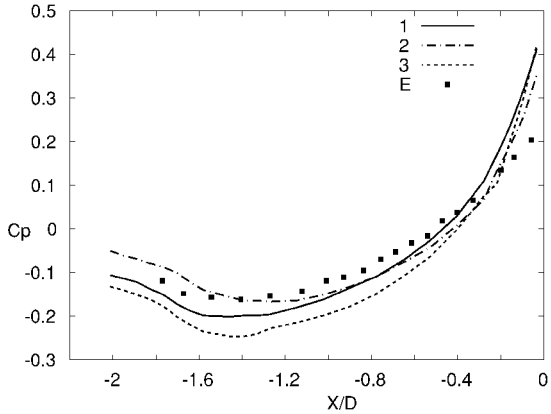

Fig. 1 AGARD WG08 test-case 1, boat-tail wall pressure coefficient: experimental data, *E* and numerical computations 1) Zannetti and Onofri and 2) and 3) other Euler computations (see Ref. 14).

Working Group WG08 (Chairman, P. Sacher) on Experimental and Computational Techniques for Aircraft Afterbodies.[14] The results of the present method on test cases 1 and 7, proposed by AGARD, are shown in Ref. 15; their comparison with experimental and other numerical results is presented in Ref. 14, in which they are identified by identification number 1. As an example, an AGARD[14] comparison between different results is presented in Fig. 1. It shows the wall pressure on the boat tail of AGARD test case 1 as computed using the present technique (denoted by 1), together with experimental results (denoted by squares) and two other numerical results.

IV. Numerical Results

A. Design of a Dual Nozzle

The first example refers to the design of a two-dimensional dual nozzle that takes the plume interactions into account. The final shape of the external nozzle is unknown, as are the shapes of the interfaces confining the inner and outer flows, and both are determined according to the inverse procedure. The computational domain is divided into two regions: 1) the inner region, which represents an internal flow bounded by the centerline, the inner nozzle contour, and the contact discontinuity, and 2) the outer region, bounded by the external nozzle walls, the contact discontinuity, and a free pressure boundary. The inner nozzle has a half-angle equal to 5 deg, and the external one has a 10-deg divergence angle. The inlet flow is supersonic for both nozzles, but with different total conditions. We have prescribed total pressure $p^0 = 1.0$, total temperature $T^0 = 1.0$, and Mach number $M = 2.0$ at the inner-nozzle inlet, and $p^0 = 0.9$, $T^0 = 1.0$, and $M = 1.8$ have been imposed at the external-nozzle inlet. The external pressure is $p_{ou} = 0.07$. Along the upper wall of the secondary nozzle, a design pressure distribution has been set according to

$$p_w = (p_{in} - p_{ou}) \sin(\pi x/1.5), \qquad 0 < x < 1.5$$
$$p_w = p_{ou}, \qquad 1.5 < x < 2.5 \tag{6}$$

where $p_{in} = 0.1566$ and $p_{ou} = 0.07$. This pressure distribution allows the secondary nozzle to be fully expanded with a nearly uniform axial flow at the exit section. The resulting flow configuration and the geometry of the secondary nozzle are shown in Figs. 2 and 3. The Mach number contour lines, plotted in Fig. 2a, reveal the presence of an embedded shock wave, generated through the coalescence of characteristics. In Fig. 2b, the pressure contours show continuous behavior across the interface. The evolution in time of the jet contour and the interface are given in Fig. 3. The initial configuration is characterized by straight lines for both the jet boundary and interface ($K = 0$). The final steady configuration is obtained after 1000 time steps.

B. Turbofan–Nacellelike Configuration

The second presented example is characterized by two evolving fluid interfaces that separate three flow regions. This is referred

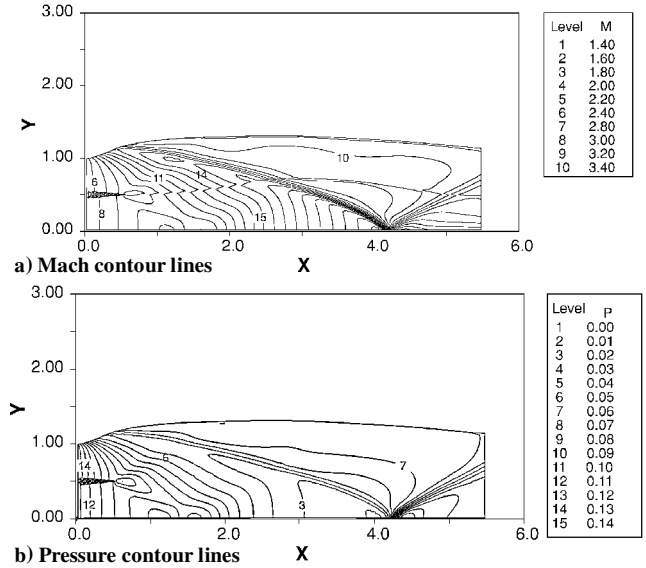

Fig. 2 Dual nozzle, final configuration.

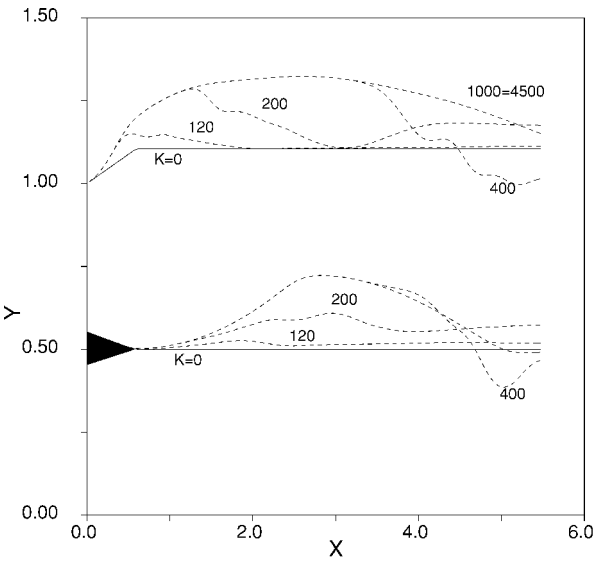

Fig. 3 Dual nozzle, plumes and outer-nozzle geometry at different time steps *K*, where *K* = 0 is initial configuration and *K* = 1000 is final geometry.

to the flow past a turbofan–nacellelike configuration because it is a schematic representation of the flowfield past a turbofan, comprehensive of the nozzles and multiple jets. The flow is assumed axisymmetric. As shown in Fig. 4, three flow regions can be identified in the afterbody flowfield as follows: 1) the region pertinent to the inner nozzle, which is bounded by the centerline, the inner nozzle contour, and the contact discontinuity that separates the hot flow from the cold flow; 2) the region pertinent to the outer nozzle, which is bounded by the mentioned contact discontinuity and a second one that separates the cold flow from the external flow; and 3) the external flowfield.

The inlet conditions imposed on the flow are the following: $P^0 = 1$ and $T^0 = 1$ in the external flow region, $P^0 = 1.3$ and $T^0 = 1.08$ in the outer-nozzle region, and $P^0 = 3.5$ and $T^0 = 1.4$ in the inner-nozzle region. The Mach number in the main flow is $M = 0.5$, which corresponds to a static pressure $p_\infty = 0.843$. The steady solution, in which the finale shape of the plumes is visible, is shown in Figs. 5–7. In terms of pressure (Fig. 5), the outer-nozzle flow recovers the external pressure value very quickly, before the inner-nozzle outlet is reached. The hot flow is characterized by an higher pressure ratio, and it accommodates itself more downstream, within

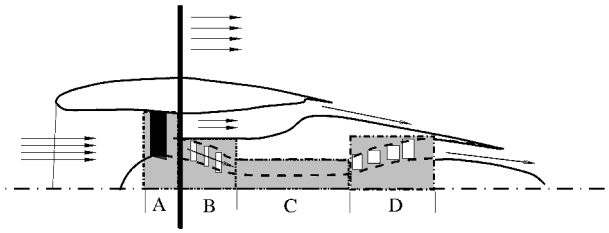

Fig. 4 Turbofan-nacelle-like configuration model: A is fan, B compressor stages, C combustor, and D turbine stages; darkened regions are black boxes. Considered computational field starts on the right of the straight vertical line between A and B.

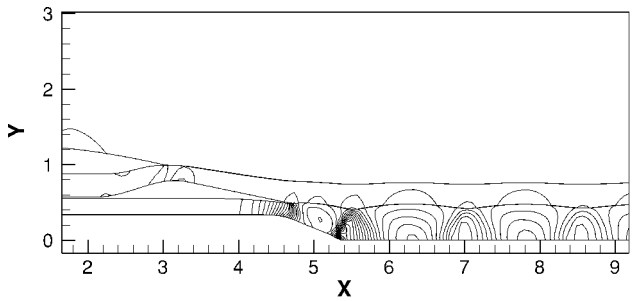

Fig. 5 Flowfield past a turbofan–nacelle-like configuration; isopressure contours.

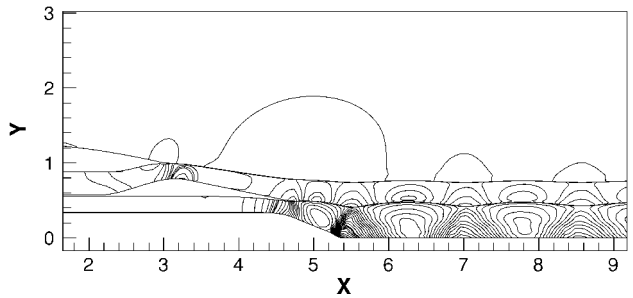

Fig. 6 Flowfield past a turbofan–nacelle-like configuration; iso-Mach contours.

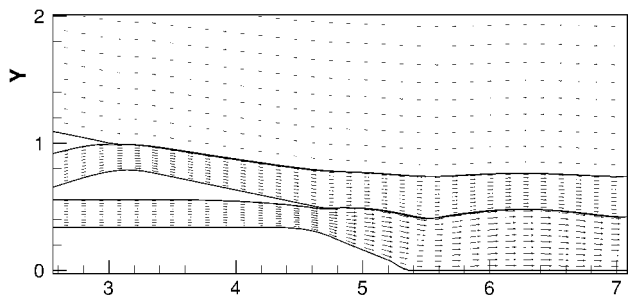

Fig. 7 Flowfield past a turbofan–nacelle-like configuration; velocity vector field.

about 3–4 inner-nozzle diameters, through repeated overcompressions and overexpansions. The wavy pattern is also visible in the Mach number isocontours (Fig. 6).

C. Ramjet Model

A two-dimensional/axisymmetric ramjet model (see Fig. 8) has been developed as an example of a complete engine system. From a modeling perspective, the ramjet is conceptually the simplest engine to work on because only a model for the burner is needed. Nevertheless, the physical scenario that has to be dealt with is very complex. Ramjet performances are very sensitive to the operating conditions of its subsystems, as well as to the external flow interactions. The flow entering the intake is supersonic, while the conditions at the burner inlet have to be subsonic. The design point in which shock-related losses are minimized coincides with the so-called shock-on-lip configuration. In short, for this configuration, an oblique shock, which departs from the inlet ramp, touches the intake lips without any inner reflection. Downstream, in the diverging channel, it is followed by a steady normal shock. The strength and position of the shock system are design variables that can be worked on to reduce losses. A heat addition model is used here to simulate the presence of the burner. Details on the flow phenomena that occur inside the burner are lost. The aim is to model only the burner effects upstream and downstream. From this point of view, the burner is a cross link between the flow leaving the inlet and the flow entering the nozzle. Despite the simplifying assumptions that have been adopted, the model allows one to take into account the complex behavior of the system as a whole. It can, therefore, give useful insights into the analysis of the flowfield at the design point as well as under offdesign conditions.

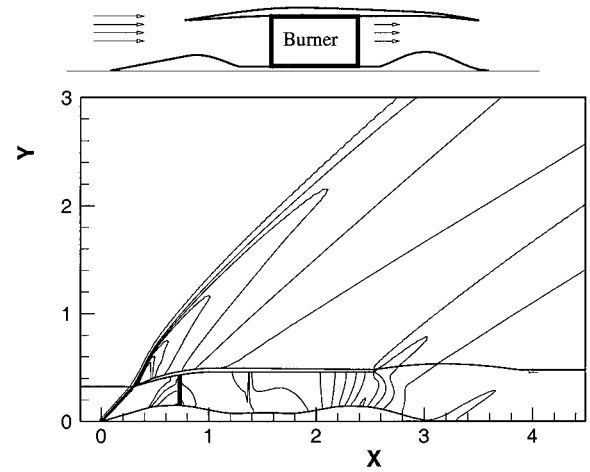

Fig. 8 Flowfield inside and around the ramjet; isopressure contours.

The presence of the burner has been simulated through an equivalent heat addition. For modeling purposes the burner is considered a cylindrical (or planar in this case) diabatic duct of constant cross area section, in which a Rayleigh flow holds. As suggested by Heiser and Pratt,[16] a total temperature distribution was postulated in the form

$$\tau(\xi) = \frac{T^0(\xi)}{T^0_{\text{bi}}} = 1 + (\tau_b - 1)\frac{\theta\xi}{1 + (\theta - 1)\xi} \tag{7}$$

where

$$\xi = \frac{x - x_{\text{bi}}}{x_{\text{bo}} - x_{\text{bi}}} \tag{8}$$

is a normalized coordinate between burner inlet x_{bi} and burner outlet x_{bo} abscissas, τ_b is the maximum allowable total temperature ratio, and $\theta > 0$ is a constant. Whatever the value of the shape parameter θ, the total enthalpy jump across the burner has to be

$$h^0_{\text{bo}} - h^0_{\text{bi}} = c_p\left(T^0_{\text{bo}} - T^0_{\text{bi}}\right) = c_p T^0_{\text{bi}}(\tau_b - 1) \tag{9}$$

The prescribed total temperature distribution $T^0_t(\xi)$ is enforced along the burner by adding to the energy equation a source term in the form

$$\dot{Q} = \rho[\gamma/(\gamma - 1)]\left[T^0_t(\xi) - T^0(\xi, t)\right](1/\Delta t) \tag{10}$$

which ensures that the correct amount of heat is added in time.

The inlet ramp angle is $\delta = 16.25$ deg. In the two-dimensional case, the inlet geometry is expected to give the shock-on-lip configuration at Mach number $M_0 = 2$. The flowfield inside and around the ramjet is shown in Figs. 8 and 9. The evolution of some fluid-dynamic quantities are presented in Fig. 10. The data have been extracted streamwise, along a central gridline.

After an external compression through the oblique shock, a steady normal shock wave is generated in the diffuser, and it ensures the necessary subsonic flow conditions at the burner inlet. The area ratio of the nozzle throat and burner gives a sonic flow only when the burner is on. To test grid sensitivity, two computations were performed on different grids with 120×54 and 240×108 nodes. The nodes in the y direction are distributed as follows: 33% to the inner flow and 66% to the outer flow. As shown in Fig. 11 no

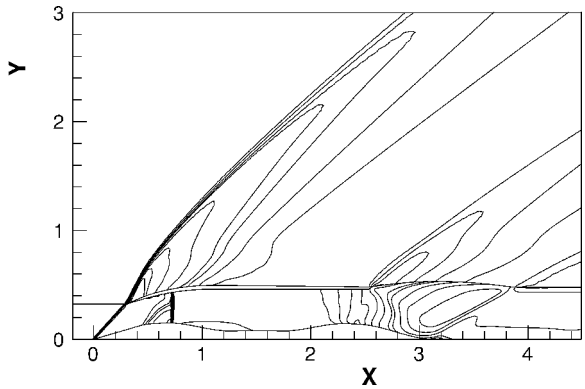

Fig. 9 Flowfield inside and around the ramjet; isomach contours.

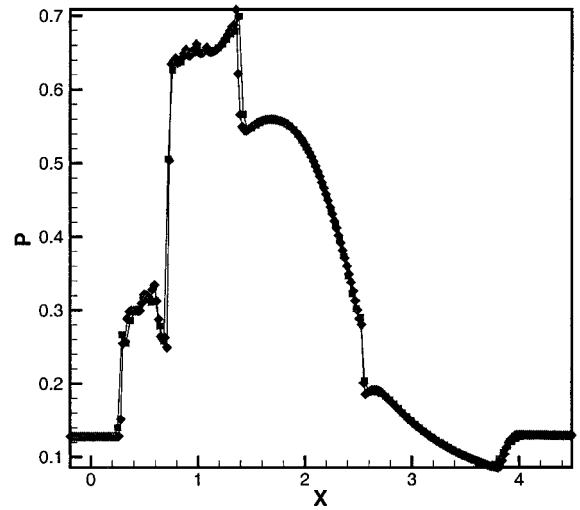

Fig. 11 Diagram of pressure along the upper wall of the ramjet and at the fluid interface: ◇, grid 120×54 and □, grid 240×108.

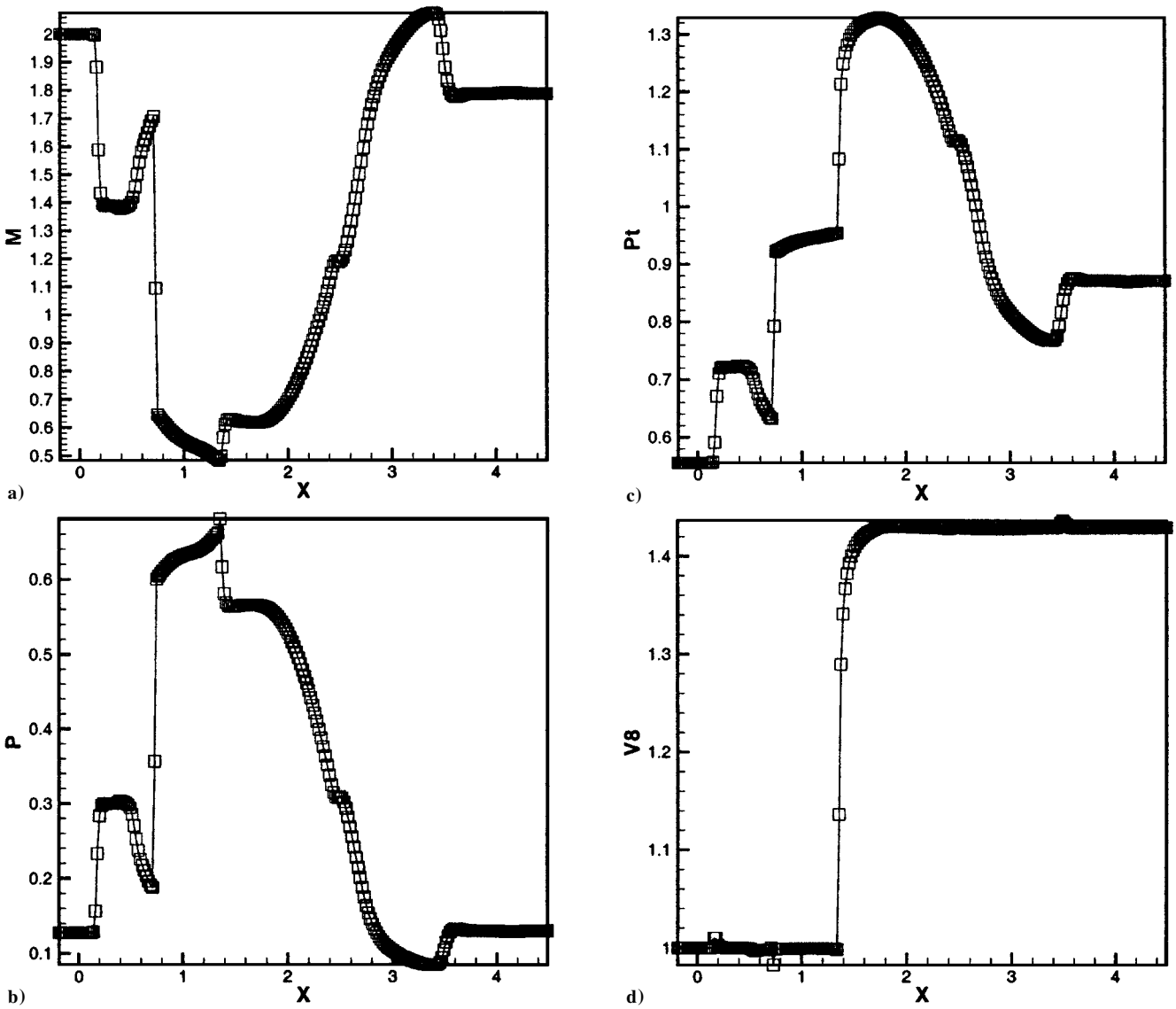

Fig. 10 Ramjet model; evolution along the streamwise direction of a) Mach number, b) static pressure, c) temperature, and d) total temperature.

appreciable differences are observed, either in the shock location or in the pressure values along the fluid interface ($x > 2.5$).

V. Conclusions

A numerical technique to design air intake and nozzles, which inherently takes into account the interaction with the external flow, has here been proposed. Coupling between the intake and the nozzles, by means of a simplified model, has been also used to simulate a complete air-breathing engine. The procedure introduces the concept of integrated design as the answer to actual requirements in the design of highly integrated engine systems, where interference between subsystems and external airflow result in a stronger coupling in the design constraints. Our modeling approach led to an inverse problem, solved in a time-dependent fashion. Several numerical examples have also been presented to explain the most important aspects of the methodology.

References

[1]Goldsmith, E. L., and Seddon, J., *Practical Intake Aerodynamic Design*, Blackwell Scientific, Boston, 1993.

[2]Mayer, D. W., and Paynter, G. C., "Prediction of Supersonic Inlet Unstart Caused by Freestream Disturbance," *AIAA Journal*, Vol. 33, No. 2, pp. 266–275.

[3]"Aspects of Engine/Airframe Integration," *Proceedings of the Seventh European Propulsion Forum*, Pau, France, March 1999.

[4]Dusa, D. J., "Exhaust Nozzle System Design Considerations for Turboramjet Propulsion Systems," *Proceedings of the Ninth International Society for Air-Breathing Engines (ISOABE) Conference*, Athens, Greece, 1989, pp. 154–160.

[5]Zannetti, L., and Larocca, F., "Inverse Methods for 3D Internal Flows," AGARD, FDP-von Kármán Inst. Special Course, Rept. 780, May 1990.

[6]Zannetti, L., "Time-Dependent Method to Solve the Inverse Problem for Internal Flows," *AIAA Journal*, Vol. 18 , No. 7, 1980, pp. 754–758.

[7]Larocca, F., and Zannetti, L., "Design Methods for Two-Dimensional Transonic Rotational Flows," AIAA Paper 95-0648, Reno, NV, Jan. 1995.

[8]Ferlauto, M., Iollo, A., and Zannetti, L., "Coupling of Inverse Methods and Optimization Techniques for Aerodynamic Shape Design," AIAA Paper 2000-0668, Reno, NV, Jan. 2000.

[9]Harten, A., Engquist, B., and Osher, S., "Uniformly High Order Accurate Essentially Non-Oscillatory Schemes III," *Journal of Computational Physics*, Vol. 71, No. 231, 1987, pp. 231–303.

[10]Di Mascio, A., and Favini, B., "A Two Step Godunov-Type Scheme for the Euler Equations," *Meccanica*, Vol. 26, No. 2/3, 1991, pp. 179–189.

[11]Pandolfi, M., "A Contribution to the Numerical Prediction of Unsteady Flows," *AIAA Journal*, Vol. 22, No. 5, 1984, pp. 602–610.

[12]Pandolfi, M., and Colasurdo, G., "Numerical Investigation on the Generation and Development of Rotating Stalls," American Society of Mechanical Engineers, ASME Paper 78-WA/GT-5, 1978.

[13]Bena, C., Larocca, F., and Zannetti, L., "Design of Multistage Axial Flow Turbines and Compressors," *Proceedings of the IMech-E 3rd European Conference on Turbomachinery*, Professional Engineering Publ., London, 1999, pp. 635–644.

[14]"Aerodynamics of Aircraft Afterbody," AGARD Rept. 226, 1986, pp. 12–219.

[15]Zannetti, L., and Onofri, M., "Aerodynamics of Aircraft After Body: Numerical Simulation," AIAA Paper 84-0284, Jan. 1984.

[16]Heiser, W. H., and Pratt, D. T., "Hypersonic Airbreathing Propulsion," *AIAA Educational Series*, AIAA, New York, 1994.